Elsevier Editorial System(tm) for Chemical Engineering Journal

Manuscript Draft

Manuscript Number:

Title: The Vis-NIR Multicolor Emitting Phosphor Ba4Gd3Na3(PO4)6F2: Eu2+, Pr3+ for LED towards Plant Growth

Article Type: Research Paper

Section/Category: Materials Synthesis and Processing

Keywords: Phosphor; Plant growth; LEDs; Energy-transfer

Corresponding Author: Professor Chongfeng Guo, Ph.D

Corresponding Author's Institution: Northwest University

First Author: Ziwei Zhou

Order of Authors: Ziwei Zhou; Niumiao Zhang; Jiayu Chen, Master; Xianju Zhou, Professor; Maxim S. Molokeev, Ph.D; Chongfeng Guo, Ph.D

Abstract: Photosynthesis process is the basic for plant growth, whcih needs energy from the light. The pigments of chlorophyll a, b and bacteriochlorophyll are responsible for the absorption of light, in which blue, red and near-infrared (NIR) light directly or indirectly promote the plant growth and enhancement of nurtiments. It is important for plant to support absorbable light, and phosphhor-converted light emitting diodes (pc-LEDs) is a low-cost, energy-saving and enviromental friendly devices for plant growth. To develop a phosphor with emission covering the blue, red and NIR, a series of phosphors Ba4Gd3Na3(PO4)6F2: Eu2+, Pr3+ with blue, red and near-infrared (NIR) multi-emitting was prepared. Their emissions not only match well with the absorption spectra of pigments in the plant, but also could be excited by near ultraviolet (n-UV) LED chip. The crystal structure of host Ba4Gd3Na3(PO4)6F2 was refined from the XRD data and three different crystallographic sites were occupied by Eu2+ determined through low temperature photoluminescence spectra. The energy transfer from Eu2+ to Pr3+ ions was also discussed in detail. Results indicated that the multi-emitting Ba4Gd3Na3(PO4)6F2: Eu2+, Pr3+ can serve as a phosphor candidate for plant growth LEDs.

Suggested Reviewers: Hongbin Liang Ph.D
Professor, School of Chemistry and Chemical Engineering, Sun Yat-sen University
cesbin@mail.sysu.edu.cn
Expert in this field.

Daqin Chen Ph.D
Professor, College of Materials & Environmental Engineering, Hangzhou Dianzi University
dqchen@hdu.edu.cn
Familiar to this field.

Hyun Kyoung Yang Ph.D
Professor, LED Convergence Engineering, Pukyong National University

hkyang@pknu.ac.kr
Familar to this field.

Opposed Reviewers:

Cover Letter

Dear editor,

On behalf of all authors, I would like to submit an electronic copy of the manuscript entitled "***The Vis-NIR Multicolor Emitting Phosphor $Ba_4Gd_3Na_3(PO_4)_6F_2$: Eu^{2+}, Pr^{3+} for LED towards Plant Growth***" for publication as an article in the ***Chemical Engineering Journal***.

Photosynthesis process is the basic for plant growth, whcih needs energy from the light. The pigments of chlorophyll a, b and bacteriochlorophyll are responsible for the absorption of light, in which blue, red and near-infrared (NIR) light is direct or indirect promote the plant growth and enhancement of nurtiments. It is an efficient method to improve crop yields and quality and tune the growth cycle of plant through synergistic effect of blue, red and NIR. It is important for plant to support absorbable light, and phosphhor-converted light emitting diodes (pc-LEDs) is a low-cost, energy-saving and enviromental friendly devices for plant growth. To develop a phosphor with emission covering the blue, red and NIR is urgent. In here, a series of phosphors $Ba_4Gd_3Na_3(PO_4)_6F_2$: Eu^{2+}, Pr^{3+} with blue, red and near-infrared (NIR) multi-emitting was prepared, their emissions not only match well with the absorption spectra of pigments in the plant, but also they could be excited by near ultraviolet (n-UV) LED chip. The crystal structure of host $Ba_4Gd_3Na_3(PO_4)_6F_2$ was refined from the XRD data and three different crystallographic sites were occupied by Eu^{2+} determing through low temperature photoluminescence spectra. The energy transfer from Eu^{2+} to Pr^{3+} ions was also discussed in detail. Results indicated that the multi-emitting $Ba_4Gd_3Na_{3(}PO_4)_6F_2$: Eu^{2+}, Pr^{3+} can serve as a phosphor candidate for plant growth LEDs.

This is why we chose your prestigious journal to present our results.

In the past one year, we have published some new results in this journal and ACS, and all of the papers have been cited ***and reviewed many times*** according to records of google scholar and ACS article views, which indicates that our research gain recognition of readers in related fields:

■Hao Suo, Xiaoqi Zhao, Zhiyu Zhang, Ting Li, Ewa M. Goldys and **Chongfeng Guo*** "Constructing Multiform Morphologies of YF_3: Er^{3+}/Yb^{3+} Up-conversion Nano/Micro-crystals towards Sub-tissue Thermometry" ***Chemical Engineering Journal 2017, 313:65-73 (Cited times 20, ESI 1%)***

■ Ziwei Zhou, Jiming Zheng, Rui Shi, Niumiao Zhang, Jiayu Chen, Ruoyu Zhang, Hao Suo, Ewa M. Goldys and **Chongfeng Guo*** "*Ab Initio* Site Occupancy and Far-red Emission of Mn^{4+} in Cubic-phased $La(MgTi)_{1/2}O_3$ for Plant Cultivation" ***ACS Applied Materials & Interfaces 2017, 9（7）：6177-6185 (Cited times 14, Article Views 494)***

■ Jiayu Chen, Niumiao Zhang, **Chongfeng Guo***, Fengjuan Pan, Xianju Zhou, Hao Suo, Xiaoqi Zhao, Ewa. M. Goldys "Site-dependent Luminescence and Thermal Stability of Eu^{2+} Doped Fluorophosphate towards White LEDs for Plant Growth" ***ACS Applied Materials & Interfaces 2016, 8(32):20856-20864 (Cited times 25, Article Views 654)***

So we believe that this time you will take into account our efforts and will give us a chance to publish in your journal. I would like to assure that our results are uniquely exceptional and the readers will definitely benefit from the results of our investigations. In addition, the article is original and never been published previously, it is not under consideration for publication elsewhere. I hope that the referees will find our research results interesting and acceptable for publication in this journal.

Thank you in advance for your consideration.

With kind regards,

Sincerely yours

Professor Chongfeng Guo

E-mail: guocf@nwu.edu.cn ;

Fax & Tel.: 086-29-88302661

List of Suggested Reviewers

Professor Hongbin Liang:

School of Chemistry and Chemical Engineering, Sun Yat-Sen University

E-mail: cesbin@mail.sysu.edu.cn

Professor Daqin Chen:

College of Materials & Environmental Engineering, Hangzhou Dianzi University

E-Mail: dqchen@hdu.edu.cn

Professor Hyun Kyoung Yang:

LED Convergence Engineering, Pukyong National University

E-mail:hkyang@pknu.ac.kr

Highlights

(1) Structure and cationic sites of sample $Ba_4Gd_3Na_3(PO_4)_6F_2$ were determined.

(2) The possibility of phosphor $Ba_4Gd_3Na_3(PO_4)_6F_2$: Eu^{2+}, Pr^{3+} with blue, red and near-infrared (NIR) emission used in plant growth LED were investigated.

*Manuscript
Click here to view linked References

The Vis-NIR Multicolor Emitting Phosphor $Ba_4Gd_3Na_3(PO_4)_6F_2$: Eu^{2+}, Pr^{3+} for LED towards Plant Growth

Ziwei Zhou[†], Niumiao Zhang[†], Jiayu Chen[†], Xianju Zhou[#], Maxim S. Molokeev[‡, Δ, ⊥, *] and Chongfeng Guo[†, *]

[†]*National Key Laboratory of Photoelectric Technology and Functional Materials (Culture Base) in Shaanxi Province, National Photoelectric Technology and Functional Materials & Application of Science and Technology International Cooperation Base, Institute of Photonics & Photon-Technology and Department of Physics, Northwest University, Xi'an 710069, China*

[#] *School of Science, Chongqing University of Posts and Telecommunications, Chongqing, 400065, P. R. China.*

[‡]*Laboratory of Crystal Physics, Kirensky Institute of Physics, Federal Research Center KSC SB RAS, Krasnoyarsk 660036, Russia*

[Δ]*Siberian Federal University, Krasnoyarsk, 660041, Russia*

[⊥]*Department of Physics, Far Eastern State Transport University, Khabarovsk, 680021 Russia*

** Author to whom correspondence should be addressed*

E-mail: guocf@nwu.edu.cn (Prof. Guo)

msmolokeev@mail.ru (Prof. Molokeev)

Tel & Fax: ±86-29-88302661

Abstract

Photosynthesis process is the basic for plant growth, whcih needs energy from the light. The pigments of chlorophyll a, b and bacteriochlorophyll are responsible for the absorption of light, in which blue, red and near-infrared (NIR) light directly or indirectly promote the plant growth and enhancement of nurtiments. It is important for plant to support absorbable light, and phosphhor-converted light emitting diodes (pc-LEDs) is a low-cost, energy-saving and enviromental friendly devices for plant growth. To develop a phosphor with emission covering the blue, red and NIR, a series of phosphors $Ba_4Gd_3Na_3(PO_4)_6F_2$: Eu^{2+}, Pr^{3+} with blue, red and near-infrared (NIR) multi-emitting was prepared. Their emissions not only match well with the absorption spectra of pigments in the plant, but also could be excited by near ultraviolet (n-UV) LED chip. The crystal structure of host $Ba_4Gd_3Na_3(PO_4)_6F_2$ was refined from the XRD data and three different crystallographic sites were occupied by Eu^{2+} determined through low temperature photoluminescence spectra. The energy transfer from Eu^{2+} to Pr^{3+} ions was also discussed in detail. Results indicated that the multi-emitting $Ba_4Gd_3Na_3(PO_4)_6F_2$: Eu^{2+}, Pr^{3+} can serve as a phosphor candidate for plant growth LEDs.

Keywords: Phosphor; Plant growth; LEDs; Energy-transfer

1. Introduction

Light guides the growth rhythm and process of plants, and the spectral composition of light environment plays a crucial role. During the typical photosynthetic process, the pigments carotenoids and chlorophylls absorb blue (400-500 nm) and red (620-690 nm) light, which directly accelerate the photosynthetic action [1-3]. However, the role of near-infrared (NIR, 715-1050 nm) light could not be omitted since it could be efficiently absorbed by bacteriochlorophyll to convert chemical energy through anaerobic photosynthesis, which promote the reproduction of photosynthetic bacteria and indirectly motivate plant growth and development [4]. It is an efficient method to improve crop yields and quality and tune the growth cycle of plant through synergistic effect of blue, red and NIR, which could be realized by appropriately adjusting the components of artificial supplying illumination source. It is more useful and necessary in a short growing season or high latitude area with poor light [5]. The commonly used incandescent and fluorescent lamps for plant illumination suffer not only spectral mismatch, but also high energy consumption or

environmental threat, whereas light-emitting diodes (LEDs) plant grow lights can overcome these shortcomings due to their high efficiency, long lifetime, environment friendly and controllable spectra composition advantages. Thus, LEDs are recognized as the first light source for plant photoreceptors to affect plant morphology and offer optimized production [6, 7].

Phosphor-converted LEDs (pc-LEDs) are the dominant product in the market due to their low cost and mature fabrication approach, which are generally fabricated by combining LED chip and phosphors [8]. Their tunable spectral components strongly depend on phosphor, thus it is urgent to design and develop a phosphor with matched spectrum with plant growth. Generally, several single color emission phosphors that can be excited efficiently by UV light have to be arranged in this scheme, leading to high cost and low luminous efficiency due to the complicated manufacture, reabsorption of emission colors and different aging rates for each phosphor. It is possible to improve the efficiency and low the cost of LEDs plant grow lamp through the application of a single phased multi-color-emitting phosphor with high chemical and thermal stability for UV-pumped LED plant growth illumination source [9].

As an typical dopant with broad excitation and emission, Eu^{2+} ions are popular activators for LED phosphors with changeable emission wavelength from near ultraviolet to near infrared due to the $4f^7 \rightarrow 4f^6 5d^1$ dipole allowed transition [10]. Because the *d*-shell electron is easily influenced by surrounding crystal-field environments, the emission wavelength of Eu^{2+} strongly depends on the strength of crystal field in the occupied sites of hosts. Apatite with the formula $A_{10}(MO_4)_6X_2$ is an important phosphor host, where A is the bivalent cation (Ca^{2+}, Ba^{2+}, Sr^{2+}, Mg^{2+}, and Pb^{2+}) or a trivalent RE^{3+} ion matching with a Na^+/K^+ ion; M is the cation (P^{5+}, Si^{4+}, Ge^{4+}, and V^{5+}); and X often represents O^{2-}, F^-, and Cl^-. A has two kinds of site: A (1) has 9-fold coordinated 4f site with C_3 symmetry, and A (2) has 7-fold coordinated 6h site with C_s symmetry (seven O atoms and two F atoms, exactly) [11]. As a member, $Ba_4Gd_3Na_3(PO_4)_6F_2$ (BGNPF): Eu^{2+} shows intense warm-white emissions centered at 485 and 570 nm under the n-UV excitation [12], which overlaps the excitation of the Pr^{3+} ion. Efficient energy transfer from Eu^{2+} ions to Pr^{3+} ions could be occurred, and the emission of Pr^{3+} covers blue ($^3P_0 \rightarrow {}^3H_4$), red ($^1D_2 \rightarrow {}^3H_4$) and NIR ($^1G_4 \rightarrow {}^3H_4$) from the spin-forbidden *f-f* transition. It is possible to obtain a single-compound phosphor with multi-band emission by co-doping Eu^{2+} ion and Pr^{3+} ion in BGNPF host [13]. Here, Eu^{2+} and Pr^{3+} ions co-doped BGNPF were synthesized *via* traditional high-temperature solid-state method

to obtain a phosphor with blue-yellow and NIR multicolor emission. The occupancy of crystallographic sites of Eu^{2+} and Pr^{3+} ions, the photoluminescence and the energy transfer from Eu^{2+} to Pr^{3+} ions were investigated in detail in this paper, which indicated that the present sample can serve as a potential phosphor for plant growth LEDs.

2. Experimental section

2.1. Materials and Synthesis.

Eu^{2+} and Pr^{3+} singly or co-doped $Ba_4Gd_3Na_3(PO_4)_6F_2$ (BGNPF) samples were prepared by a traditional high-temperature solid-state method, in which the stoichiometric amount of analytical reagent (A. R.) raw materials $BaCO_3$, Na_2CO_3, $NH_4H_2PO_4$, BaF_2 and high purity Gd_2O_3 (99.99%), Eu_2O_3 (99.99%) and Pr_6O_{11} (99.99%) were first weighted and mixed with an alcohol in evaporating dish. After that, the dish with raw materials was transferred into an oven to dry at 70 °C for 2 h and then thoroughly ground the powder for 20 minutes in an agate mortar. The mixture powders were pre-heated in furnace at 500 °C for 5 h and subsequently sintered at 1075 °C for 6 h in reducing atmosphere to get the final samples.

2.2. Characterization and calculation.

The powder X-ray diffraction (XRD) data of $Ba_4Gd_3Na_3(PO_4)_6F_2$ for Rietveld analysis were collected at room temperature with a Bruker D8 ADVANCE powder diffractometer (Cu-Kα radiation) and linear VANTEC detector. The step size of 2θ was 0.016°, and the counting time was 2 s per step. Rietveld refinement was performed by using TOPAS 4.2 [14]. The photoluminescence emission (PL) and excitation (PLE) of phosphors as well as decay curves were measured on an Edinburgh FLS920 fluorescence spectrophotometer (Edinburgh Instruments Ltd., UK) equipped with a 450W Xe lamp and EPL-375 picosecond pulsed diode laser (Edinburgh Instruments Ltd.) as excitation source. An oxford OptistatDN2 nitrogen cryogenics temperature controlling system was combined with spectrophotometer to measure the temperature-dependent PL spectra and duration of staying at the measured temperature was 10 minutes.

3. Results and discussion

3.1 The phase purity and crystal structure

The XRD pattern of blank phosphor BGNPF is shown in Fig. 1a, it's found that almost all diffraction peaks are indexed to trigonal cell (*P*-3) with parameters close to $Ba_4Nd_3Na_3(PO_4)_6F_2$

[15] (apatite-type structure, JCPDS# 71-1318) except few peaks from trace impurity $Na_3Gd(PO_4)_2$ (wt. = 5.9(4)%, as shown in the inset of Fig. 1a). Therefore, the crystal structure of $Ba_4Nd_3Na_3(PO_4)_6F_2$ is taken as original model for Rietveld refinement, and the Nd ion site is occupied by Gd ion, refinement is stable with low *R*-factors (shown in Tab. 1). The cell parameters of hexagonal fluorophosphates BGNPF with space group *p*-3 are $a = b = 9.7477(3)$ Å, $c = 7.2220(3)$ Å, $V = 594.27(4)$ Å^3. According to refinement result, the crystal structure of BGNPF is shown in Fig. 1b, in which there are one Ba^{2+} site and two kinds of Gd^{3+} cationic crystallographic sites in BGNPF. The coordination polyhedron of Ba and Gd (1) is coordinated by seven oxygens and two fluorides, coordination number (CN) is 9, and Gd (2) is coordinated by nine oxygens, which indicates that three cationic sites offer different crystal field environment for Eu^{2+}. Considering the similar ionic radii of dopant Eu^{2+} (r = 1.30 Å, CN = 9), Pr^{3+} (r = 1.319 Å, CN = 9) and cationic ions Ba^{2+} (r = 1.47 Å, CN = 9) or Gd^{3+} (r = 1.247 Å, CN = 9) in host, it's possible for Eu^{2+} and Pr^{3+} ions to randomly enter the sites of Ba^{2+} and Gd^{3+} [12].

3.2 The photoluminescent property of BGNPF: Eu^{2+} phosphor

The emission wavelength of Eu^{2+} strongly depends on the crystal field environment of the occupied sites because its typical $5d \rightarrow 4f$ transition. To identify the occupancy of Eu^{2+} in host $Ba_4Nd_3Na_3(PO_4)_6F_2$, the emission and excitation spectra of BGNPF: Eu^{2+} at liquid helium temperature (LHT) were shown in Fig. 2a. It is observed that the PL spectrum is consist of a broad asymmetric emission band covering the region of 400 to 800 nm from the transition of Eu^{2+} $4f^6 5d^1 \rightarrow 4f^7$ along with a small sharp peak at 615 nm from the $^5D_0 \rightarrow {}^7F_2$ transition of unreduced Eu^{3+} under the excitation of 365 nm n-UV light. The former can be decomposed into three Gaussian peaks centered at 446, 484, and 593 nm, respectively, which implies that Eu^{2+} ions occupy three different sites. According to the above structure analysis results, there are three cationic sites Ba, Gd (1), and Gd (2) can be occupied by Eu^{2+} ions in the BGNPF host. For the same nine-coordination environment, the average bond length Ba/Gd (1)-O (~2.726 Å) (7O, 2F) is distinctly longer than that of Gd (2)-O (~2.453 Å) (9O), which means that the crystal field strength of Ba/Gd (1) site is weaker than that of Gd (2) site [16]. Thus, the emission band centered at 593 nm is assigned to Eu^{2+} ions located at Gd (2) site with stronger crystal field; whereas the emission of Eu^{2+} occupied the Ba site must be close to that of Gd (1) site due to their similar coordination

environments. On the basis of previous discussion by Van Uitert [17], the environment- dependent emission position of Eu^{2+} ions can be evaluated by following equation [18]:

$$E = Q\left[1 - \left(\frac{V}{4}\right)^{\frac{1}{V}} \times 10^{-nE_a r/80}\right] \quad (3)$$

where E is the position of the d-band edge in energy for Eu^{2+} ion (cm^{-1}), Q is the position of the d-band edge in energy for free ion (Q = 34000 for Eu^{2+}), V is the valence of the activator (V = 2 for Eu^{2+}), n is the coordination number of activator, r is the ion radii of the occupied cation by activator in the host, E_a is a constant for the same host and defined to be 1 by us to simplify the operation. In light of the *Eq*. (3), the E(Gd (1)) = 17572.78 > 15950.55 = E(Ba), which means the emission centered at 446 and 484 nm was attributed to entered the Eu^{2+} entered the sites of Ba and Gd (1), respectively. In sum up, the three emission bands at 446, 484 and 593 nm are assigned to activators Eu^{2+} occupied the sites of Ba, Gd (1) (coordinated with 7O and 2F) and Gd (2) site (coordinated with 9O), respectively. For the PLE spectra of BGNPF: Eu^{2+} at LHT monitored at 446, 484, and 593 nm, clearly difference were observed though typical intense absorption broad bands from 250 to 450 nm assigned to the $4f^7 \rightarrow 4f^6 5d^1$ transition of Eu^{2+} appeared [19]. The sharp line absorption peaks belong to the $^7F_0 \rightarrow {}^5D_4$, $^5L_7$, $^5L_6$ transitions of Eu^{3+} were found in the PLE spectra monitored at 484 and 593 nm whereas no sharp peaks presented in the PLE spectrum monitored at 446 nm, which further improve that it is difficult be completely reduced to Eu^{2+} for Eu^{3+} occupied the Gd^{3+} site owing to the imbalance valence state.

By contrast, the sharp line emission for the unreduced Eu^{3+} disappeared and the dominant emission band obviously shifts to blue region in the PL spectra of BGNPF: Eu^{2+} at room temperature (in Fig. 2b). However, it could overlap with the absorption of carotenoid, chlorophyll a and b with the excitation of 365 nm near ultraviolet light, which indicated that the prepared phosphors BGNPF: Eu^{2+} could be used in the plant growth LEDs. To determine the optimal composition of the phosphor, the PL profiles of BGNPF: $x$$Eu^{2+}$ were presented in Fig. 2c as a function of Eu^{2+} concentration under the excitation of 340 nm. It is observed that the PL intensity first gradually increase and then declines after reaching the maximum value at x = 0.9% due to the concentration quenching resulting from the shorter and shorter distance between identical Eu^{2+} ions in the crystal host. The critical distance (R_c) can be estimated by the following formula [20]:

$$R_c = 2\left[\frac{3V}{4\pi x_c N}\right]^{1/3} \quad (1)$$

where V is the volume of the unit cell, N is the number of host cations in the unit cell, and x_c is the critical concentration of Eu^{2+} ions. The calculated critical distance (R_c) is about 26.21 Å according to the V = 594.27(4) $Å^3$, N = 7, and x_c = 0.009, which is far beyond 5 Å and means that the energy transfer among Eu^{2+} ions is not controlled by exchange interaction mechanism which generally occurred in a forbidden transition. Moreover, the inapparent overlap between the excitation and emission spectra hints that the electric multipolar interaction energy transfer is responsible for the concentration quenching, and the type of interaction can be described by following equation [21, 22]:

$$\frac{I}{x} = K\left[\frac{1}{1+\beta(x)^{\theta/3}}\right] \quad (2)$$

where I is the PL intensity, x is the activator concentration over the critical concentration, K and β are constants for the same excitation condition and host lattice. θ = 3, 6, 8, or 10 representative the non-radiative energy transfer mechanism of exchange coupling, dipole-dipole (d-d), dipole-quadrupole (d-q), and quadrupole-quadrupole (q-q) interactions, respectively. The slop of well-fitted straight line on the basis of Ln(I/x) *vs* Ln(x) is -1.55 (-θ/3), as shown in Fig. 2d. The value of θ is calculated to be 4.65 in the middle of 3 and 6, which indicates that the exchange coupling and d-d interaction mechanism collectively dominate the concentration quenching effect in BGNPF: Eu^{2+}.

For the practical application of phosphor in LEDs, its thermal stability is a vital parameter owing to about 150 °C operating temperature of LED chip [9]. The intensity map of temperature-dependent PL spectra of BGNPF: 0.9%Eu^{2+} phosphor with optimal composition is displayed in Fig. 3a, it is found that the intensity of the phosphor decreases gradually with increasing the temperature. Meanwhile, the descent speed of PL intensity in yellow region is faster than that in blue region, which further proves that yellow and blue emission come from different luminescence centers Eu^{2+} occupied different cationic sites in the host. The normalized integrated intensities (400-800 nm) of BGNPF: 0.9%Eu^{2+} was also given in Fig. 3b as a function of heating temperature from 298 to 498 K, the integrated PL intensity decreases with increasing temperature and reach about 37.3% of the initial intensity at 423 K. The thermal activation energy ΔE_a can be calculated according to following equation [23]:

$$I(T) = \frac{I(0)}{1+cexp(-\Delta E_a/k_B T)} \quad (4)$$

where *I(0)* is the initial emission intensity at room temperature, *I(T)* is the emission intensity at temperature *T*, *c* is a constant, ΔE_a is thermal activation energy, *K* is the Boltzmann constant (K = 8.62×10^{-5} eV). The data are well fitted by the plot of $\ln(I_0/I\text{-}1)$ *vs* $10000/T$ in the Fig. 3c, and the thermal activation energy ΔE_a is calculated to be 0.29 eV. Furthermore, it is noteworthy that the blue emission peak (485 nm) shows a slight shift with heating from 298 to 498 K, which is due to the thermally active phonon-assisted tunneling from the excited states of the low-energy emission band to those of the higher energy emission band. With the increase of temperature, the probability of this effect persistently enhanced and the emission energy become higher and higher, which is reflected in the blue shift of temperature-dependence spectra [24].

3.3 The energy transfer of Eu^{2+} → Pr^{3+} in BGNPF: Eu^{2+}, Pr^{3+} phosphor

NIR light not only could indirectly promote the plant growth but also could enhance the nutriments in food, which is as indispensable as blue and red light. The emission of Pr^{3+} covers the blue, red and NIR region, which is an important activator for plant growth phosphor. However, narrow absorption cross-section of Pr^{3+} from the spin-forbidden *f-f* transitions leads to its low efficiency, which can be greatly enhanced through introduction efficient sensitizer. Generally, the significant overlap between the emission spectra of sensitizer and the excitation of Pr^{3+} is necessary. The PLE and PL spectra of Eu^{2+} and Pr^{3+} solely doped BGNPF are shown in Fig. 4a and b, respectively. A strong and broad absorption belonging to the $4f^7 \rightarrow 4f^6 5d^1$ transition of Eu^{2+} and emission band ranging from 400 to 800 nm from Eu^{2+} were observed in BGNPF: Eu^{2+} (in Fig. 4a); whereas the excitation spectrum of BGNPF: Pr^{3+} consists of several line absorption at 447, 470, and 484 nm from the ground level $^3H_4$ to $^3P_2$, $^3P_1$ and $^3P_0$ levels transitions of Pr^{3+} ion, the PL spectrum includes strong red and NIR emission. Comparing Fig. 4a and b, an obvious overlap between the PL spectra of Eu^{2+} and the PLE spectra of Pr^{3+} was observed, which indicate that the efficient energy transfer from Eu^{2+} to Pr^{3+} is expected to occur in the Eu^{2+}-Pr^{3+} co-doped BGNPF.

The PLE and PL spectra of BGNPF: 0.9%Eu^{2+}, 1%Pr^{3+} phosphor are shown in Fig. 4c, the PLE spectra monitored at 570 nm (Eu^{2+}: $4f^6 5d^1 \rightarrow 4f^7$) and 1022 nm ($Pr^{3+}$: $^1G_4 \rightarrow {}^3H_4$) are similar except a group of sharp lines absorption from Pr^{3+} in the latter, but they all includes the typical broad band (250 - 450 nm) absorption from Eu^{2+}, which further confirm the occurrence of the

energy transfer from Eu^{2+} to Pr^{3+} ion. Under the 365 nm excited, the PL spectrum of phosphor BGNPF: 0.9%Eu^{2+}, 1%Pr^{3+} composes of a broad band emission in visible region and a group of sharp lines emission peaked at 601 and 1022 nm from Eu^{2+} and Pr^{3+}, respectively. The integrated emission intensity in visible and NIR region of samples BGNPF: 0.9%Eu^{2+}, *y*Pr^{3+} were offered in the inset of Fig. 4c as a function of Pr^{3+} concentration in the range of 0.5~ 3.0%, in which the visible emission intensity monotonously decreases whereas the NIR emission intensity first goes up and then declines with the increase of Pr^{3+} concentration due to the energy transfer from Eu^{2+} to Pr^{3+} and concentration quenching effect [25]. It is found that the emission spectra of BGNPF: Eu^{2+}, Pr^{3+} covers blue, red and NIR region, which match well with the absorption spectra of carotenoid, chlorophyll a, b and bacteriochlorophyll and implies that the prepared phosphor can be used in the plant growth LEDs.

To further testify the ET process from Eu^{2+} to Pr^{3+} ions in BGNPF: Eu^{2+}, Pr^{3+}, the decay curves and corresponding lifetime of Eu^{2+} in BGNPF: 0.9%Eu^{2+}, *y*Pr^{3+} phosphors (monitored at 485 nm) are exhibited in Fig. 5a. The decay curves can be well fitted with a second-order exponential as following equations [26, 27]:

$$I_\tau = I_0 + A_1 \exp\left(-\frac{t}{\tau_1}\right) + A_2 \exp\left(-\frac{t}{\tau_2}\right) \quad (5)$$

$$\tau^* = \frac{A_1\tau_1^2 + A_2\tau_2^2}{A_1\tau_1 + A_2\tau_2} \quad (6)$$

where I_t and I_0 are the luminescence intensity as time are 0 and *t*, A_1 and A_2 are constants, τ_1 and τ_2 are the fast and slow lifetimes, respectively. τ^* is the effective lifetime. According to the *Eq.* (5) and (6), the τ^* is about 448, 445, 382, 371, and 298 ns for *y* = 0.0%, 0.5%, 1.0%, 1.5%, and 2.0%, respectively. Obviously, the lifetimes of Eu^{2+} ions gradually decrease with the increase of Pr^{3+} concentration (as shown in Fig. 5b), which can further confirm the existence of energy transfer from Eu^{2+} to Pr^{3+} ions. The energy transfer efficiency (η_τ) from Eu^{2+} to Pr^{3+} ions in the BGNPF: Eu^{2+}, Pr^{3+} are calculated according to the life time of Eu^{2+} based on the following equation [28]:

$$\eta_\tau = 1 - \frac{\tau}{\tau_0} \quad (7)$$

where τ_0 and τ stand for the decay lifetimes of the samples without and with the Pr^{3+} ions, respectively. The τ and η_τ are plotted as a function of the Pr^{3+} concentration and displayed in Fig. 5c, in which the ET efficiency from Eu^{2+} to Pr^{3+} rises gradually with the growth of Pr^{3+} concentration.

To further explain the energy transfer process, the energy level schematic diagram is presented in Fig. 6. When excited by 220-450 nm, the electrons in the *4f* ground state can be bumped to the *5d* excited state, and then relaxed to the lowest excited state through non-radiative relaxation. There are two ways for Eu^{2+} ions to transfer their absorbed energy to Pr^{3+} ion, one is the part of excited electrons go back to the ground state *4f* and give a broadband emission centered at 485 nm, then part of the emission energy is reabsorbed by Pr^{3+} to pump the electrons from $^3H_4$ to $^3P_{0, 1, 2}$. The other energy transfer process is part of electrons at the excited *5d* level of Eu^{2+} directly transfer to the neighbor Pr^{3+} ions due to their close excited energy levels. Therefore, energy transfer from Eu^{2+} to Pr^{3+} is the main pathway to populate the excited states $^3P_{0, 1, 2}$ and $^1I_6$ levels of Pr^{3+}. Then the electrons at $^3P_2$ level non-radiative relax to the lower $^3P_1$ and $^3P_0$ levels, resulting visible emission peaks at 526 ($^3P_1 \rightarrow {}^3H_5$), 596 ($^3P_1 \rightarrow {}^3H_6$), 601 ($^1D_2 \rightarrow {}^3H_4$), 610 ($^3P_1 \rightarrow {}^3H_6$) and 644 ($^3P_0 \rightarrow {}^3F_2$) nm. In addition, phonon-assisted non-radiative relaxation (NR) from $^3P_0$ to $^1D_2$ level and cross-relaxation (CR) CR1 ($^3P_0 + {}^3H_6 \rightarrow {}^3H_4 + {}^1D_2$) and CR2 ($^3P_0 + {}^1D_2 \rightarrow {}^3H_4 + {}^3H_6$) also participate at high concentration and result in concentration quenching process. The energy gap between $^3P_0$ and $^1D_2$ is 3866 cm^{-1} and the maximum vibrational frequency of phosphate is 1037 cm^{-1}, so the non-radiation (NR) process may come up with 3~4 phonons assisted [26]. Therefore, the CR process plays an more important role in populating electrons to $^1D_2$ energy level than that of NR process, so the red emission at 601 nm ($^1D_2 \rightarrow {}^3H_4$) and NIR emission 865 nm ($^1D_2 \rightarrow {}^3F_2$) are relatively stronger. At the same time, the electrons will populate to the $^1G_4$ energy level through CR3 ($^1D_2 + {}^1G_4 \rightarrow {}^3H_4 + {}^3F_4$), and then radiative back to the ground state $^3H_4$ with 1022 nm ($^1G_4 \rightarrow {}^3H_4$) NIR emission. Furthermore, when electrons populate to the $^3P_0$ energy level, the NIR two photon emissions ($^3P_0 \rightarrow {}^1G_4 \rightarrow {}^3H_4$) may occur by assimilating a visible photon and emitting two NIR photons, so the 916 ($^3P_0 \rightarrow {}^1G_4$) and 1022 ($^1G_4 \rightarrow {}^3H_4$) nm NIR light can be observed in the test [29]. Just as shown in Fig. 2b, the intensity of the peak at 916 nm is incredibly weaker than that of 1022 nm, which indicates that the possible of NIR two photon emissions is very slim. Therefore, the NIR emission is closely linked CR and NR process.

4. Conclusion

In summary, a series of Eu^{2+}-Pr^{3+} co-doped apatite phosphors $Ba_4Gd_3Na_3(PO_4)_6F_2$: Eu^{2+}, Pr^{3+} used

for plant growth LEDs were successfully synthesized by the traditional high-temperature solid-state method in a reduced atmosphere. The crystal structure of host $Ba_4Gd_3Na_3(PO_4)_6F_2$ were determined through the refinement of XRD, in which three crystallographic sites were offered for the occupency of Eu^{2+} and the assignment of three broad band emission at 446, 484 and 593 nm contributed to Eu^{2+} at the sites of Ba, Gd (1) (coordinated with 7O and 2F) and Gd (2) site (coordinated with 9O) through spectra at liquid helium temperature. The energy transfer process from Eu^{2+} to Pr^{3+} were confirmed through the overlap of PL spectrum of BGNPF: Eu^{2+} and PLE spectrum of BGNPF: Pr^{3+} and the decrease of Eu^{2+} average lifetime in BGNPF: Eu^{2+}, Pr^{3+} with raising the concentration of Pr^{3+}. The present sample BGNPF: Eu^{2+}, Pr^{3+} not only offers a strong and broad absorption band ranging from 220 to 420 nm but also exhibits blue, red and NIR emission, which implies that the emission spectra of the sample match well with the absorption spectra of pigments carotenoids, chlorophyll a, b and bacteriochlorophyll in plant with the excitation of n-UV light. Results indicate that the present phosphor BGNPF: Eu^{2+}, Pr^{3+} shows great potential for plant growth LEDs.

Acknowledgments

This work was supported by National Natural Science Foundation of China (No. 11704312, 11274251), Research Fund for the Doctoral Program of Higher Education of China (RFDP) (No.20136101110017), Foundation of Key Laboratory of Photoelectric Technology in Shaanxi Province (15JS101).

References

[1] C. C. Lin, A. Meijerink, R. S. Liu, Critical Red Components for Next-Generation White LEDs, J. Phys. Chem. Lett. 7 (2016) 495-503.

[2] Z. W. Zhou, J. M. Zheng, R. Shi, N. M. Zhang, J. Y. Chen, R. Y. Zhang, H. Suo, E. M. Goldys, C. F. Guo, Ab initio Site Occupancy and Far-Red Emission of Mn^{4+} in Cubic-Phase $La(MgTi)_{1/2}O_3$ for Plant Cultivation, ACS Appl. Mater. Inter. 9 (2017) 6177-6185.

[3] J. Y. Chen, N. M. Zhang, C. F. Guo, F. J. Pan, X. J. Zhou, H. Suo, X. Q. Zhao, E. M. Golys, Site-Dependent Luminescence and Thermal Stability of Eu^{2+} Doped Fluorophosphate toward White LEDs for Plant Growth, ACS Appl. Mater. Inter. 8 (2016) 20856-20864.

[4] N. Yeh, J. P. Chung, High-brightness LEDs-Energy Efficient Lighting Sources and Their

Potential in Indoor Plant Cultivation, Renew. Sust. Energ. Rev. 13 (2009) 2175-2180.

[5] V. F, A mechanistic view of the capacity of forests to cope with climate change, Managing forest ecosystems: the challenge of climate change, Springer-Verlag Berlin and Heidelberg, Cham, 2017.

[6] Z. Y. Mao, J. J. Chen, D. J. Wang, Dual-Responsive Sr_2SiO_4: Eu^{2+}-$Ba_3MgSi_2O_8$: Eu^{2+}, Mn^{2+} Composite Phosphor to Human Eyes and Plant Chlorophylls Applications for General Lighting and Plant Lighting, Chem. Eng. J. 284 (2016), 1003-1007.

[7] G. D. Massa, H. H. Kim, R. M. Wheeler, C. A. Mitchell, Plant Productivity in Response to LED Lighting, Hortscience 43 (2008) 1951-1956.

[8] M. M. Shang, C. X. Li, J. Lin, How to Produce White Light in a Single-Phase Host?, Chem. Soc. Rev. 43 (2014) 1372-1386.

[9] C. F. Guo, H. Suo, Design of single-phased multicolor-emission phosphor for LED Phosphors, Up Conversion Nano Particles, Quantum Dots and Their Applications, Springer-Verlag Berlin and Heidelberg, Ch, 2017.

[10] M. M. Shang, S. S. Liang, N. R. Qu, H. Z. Lian, J. Lin, Influence of Anion/Cation Substitution ($Sr^{2+}\rightarrow Ba^{2+}$, $Al^{3+}\rightarrow Si^{4+}$, $N^{3-}\rightarrow O^{2-}$) on Phase Transformation and Luminescence Properties of $Ba_3Si_6O_{15}$: Eu^{2+} Phosphors, Chem. Mater. 29 (2017) 1813-1829.

[11] W. J. Zhou, F.J. Pan, L. Zhou, D. J. Hou, Y. Huang, Y. Tao, H. B. Liang, Site Occipancies, Luminescence, and Thermometric Properties of $LiY_9(SiO_4)_6O_2$: Ce^{3+} Phosphors, Inorg. Chem. 55 (2016) 10415-10424.

[12] X. P. Fu, W. Lü, M. M. Jiao, H. P. You, Broadband Yellowish-Green Emitting $Ba_4Gd_3Na_3(PO_4)_6F_2$: Eu^{2+} Phosphor: Structure Refinement, Energy Transfer, and Thermal Stability, Inorg. Chem. 55 (2016) 6107-6113.

[13] A. Huang, Z. W. Yang, C. Y. Yu, Z. H. Chai, J. B. Qiu, Z. G. Song, Tunable and White Light Emission of a Single-Phased $Ba_2Y(BO_3)_2Cl$: Bi^{3+}, Eu^{3+} Phosphor by Energy Transfer for Ultraviolet Converted White LEDs, J. Phys. Chem. C 121 (2017) 5267-5276.

[14] Bruker AXS TOPAS V4: General Profile and Structure Analysis Software for Powder Diffraction data. – User's Manual. Bruker AXS, Karlsruhe, Germany, 2008.

[15] M. Mathew, I. Mayer, B. Dickens, L.W. Schroeder, Substitution in Barium-Fluoride Apatite: the Crystal Structures of $Ba_{10}(PO_4)_6F_2$, $Ba_6La_2Na_2(PO_4)_6F_2$ and $Ba_4Nd_3Na_3(PO_4)_6F_2$, J. Solid State

Chem. 28 (1979) 79-95.

[16] Y. C. Wang, J. Y. Ding, Y. Y. Li, X. Ding, Y. H. Wang, Preparation, crystal structure and photoluminescence properties of Ce^{3+} activated $Ba_3Y_{1-y}Lu_yAl_2O_{7.5}$phosphors for near-UV LEDs, Chem. Eng. J. 315 (2017) 382-391.

[17] L. G. Van Uitert, An Empirical Relation Fitting the Position in Energy of the Lower d-Band Edge for Eu^{2+} or Ce^{3+} in Various Compounds, J. Lumin. 29 (1984) 1-9.

[18] J. M. Wang, H. Lin, Q. M. Huang, G. C. Xiao, J. Xu, B. Wang, T. Hu, Y. S. Wang, Structure and Luminescence behavior of A Single-ion Activated Single-phased $Ba_2Y_3(SiO_4)_3F$: Eu White-Light Phosphor, J. Mater. Chem. C 5 (2017) 1789-1797.

[19] S. P. Lee, T. S. Chan, T. M. Chen, Novel Reddish-Orange-Emitting $BaLa_2Si_2S_8$: Eu^{2+} Thiosilicate Phosphor for LED Lighting, ACS Appl. Mater. Inter. 7 (2015) 40-44.

[20] W. Z. Sun, Y. L. Jia, R. Pang, H. F. Li, T. F. Ma, D. Li, J. P. Fu, S. Zhang, L. H. Jiang, C. Y. Li, $Sr_9Mg_{1.5}(PO_4)_7$: Eu^{2+}: A Novel Broadband Orange-Yellow-Emitting Phosphor For Blue Light-Excited Warm White LEDs, ACS Appl. Mater. Inter. 7 (2015) 25219-25226.

[21] L. G. Van Uitert, Characterization of Energy Transfer Interactions between Rare Earth Ions, J. Electrochem. Soc. 114 (1967) 1048-1053.

[22] X. Y. Liu, H. Guo, Y. Liu, S. Ye, M. Y. Peng, Q. Y. Zhang, Thermal Quenching and Energy Transfer in Novel Bi^{3+}/Mn^{2+} Co-doped White-emitting Borosilicate Glasses for UV LEDs, J. Mater. Chem. C 4 (2016) 2506-2512.

[23] P. P. Dai, C. Li, X. T. Zhang, J. Xu, X. Chen, X. L. Wang, Y. Jia, X. J. Wang, Y. C. Liu, A Single Eu^{2+}-Activated High-Color-Rendering Oxychloride White-Light Phosphor for White-Light-Emitting Diodes, Light: Sci. Appl. 5 (2016) e16024.

[24] Z. Y. Zhao, Z. G. Yang, Y. R. Shi, C. Wang, B. T. Liu, G. Zhu, Y. H. Wang, Red-Emitting Oxonitridosilicate phosphors $Sr_2SiN_zO_{4-1.5z}$: Eu^{2+} for White Light-Emitting Diodes: Structure and Luminescence Properties, J. Mater. Chem. C 1 (2013) 1407-1412.

[25] H. J. Guo, Y. H. Wang, G. Li, J. Liu, P. Feng, D. W. Liu, Cyan Emissive Super-Persistent Luminescence and Thermoluminescence in $BaZrSi_3O_9$: Eu^{2+}, Pr^{3+} phosphors , J. Mater. Chem. C 5 (2017) 2844-2851.

[26] J. Y. Chen, C. F. Guo, Z. Yang, T. Li, J. Zhao, Li_2SrSiO_4: Ce^{3+}, Pr^{3+}Phosphor with Blue, Red, and Near-Infrared Emission Used for Plant Growth LED, J. Am. Ceram. Soc. 99 (2016) 218-225.

[27] H. Suo, C. F. Guo, T. Li, Broad-Scope Thermometry Based on Dual-Color Modulation Up-Conversion Phosphor $Ba_5Gd_8Zn_4O_2$: Er^{3+}/ Yb^{3+}, J. Phys. Chem. C 120 (2016) 2914-2924.

[28] P. L. Li, Z. J. Wang, Z. P. Yang, Q. L. Guo, A Novel, Warm, White Light-Emitting phosphor Ca_2PO_4Cl: Eu^{2+}, Mn^{2+} for white LEDs, J. Mater. Chem. C 2 (2014) 7823-7829.

[29] Y. Chen, J. Wang, C. M. Liu, J. K. Tang, X. J. Kuang, M. M. Wu, Q. Su, UV-Vis-NIR Luminescence Properties and Energy Transfer Mechanism of $LiSrPO_4$: Eu^{2+}, Pr^{3+} Suitable for Solar Spectral Convertor, Opt. Express 21 (2013) 3161-3169.

Figure captions

Figure 1. (a) Difference Rietveld plot of $Ba_4Gd_3Na_3(PO_4)_6F_2$ with small amount of $Na_3Gd(PO_4)_2$ impurity; (b) Crystal structure of $Ba_4Gd_3Na_3(PO_4)_6F_2$.

Figure 2. (a) The PLE (λ_{em} = 446, 484, 593 nm) and PL (λ_{ex} = 365 nm) spectra of BGNPF: Eu^{2+} at 10 K and (b) the PL spectra of BGNPF: Eu^{2+} at room temperature; (c) The Eu^{2+} contents-dependent PL spectra of BGNPF: x%Eu^{2+} (x = 0.5%-10.0%) and (d) The dependence of ln(I/x) on ln(x). The inset of (b) is the absorb spectra of carotenoid, chlorophyll a and b.

Figure 3. Intensity map of temperature-dependent PL spectra (a) and the corresponding normalized the integrated (400-800 nm) intensity (b) as well as the plot of In(I_0/I-1) *vs* 10000/T (c) for sample BGNPF: 0.9%Eu^{2+}.

Figure 4. The PLE and PL spectra of (a) BGNPF: 0.9%Eu^{2+}, (b) BGNPF: 1%Pr^{3+} and (c) BGNPF: 0.9%Eu^{2+}, 1%Pr^{3+}.Inset is the Pr^{3+} contents-dependent integral intensity of BGNPF: 0.9%Eu^{2+}, y%Pr^{3+} samples in visible and NIR region.

Figure 5. (a) The decay curves, (b) decay time of Eu^{2+} and (c) energy transfer efficiency from Eu^{2+} to Pr^{3+} in phosphor BGNPF: 0.9%Eu^{2+}, y%Pr^{3+}as function of Pr^{3+} concentration.

Figure 6. Schematic energy level diagram and the energy transfer process among Eu^{2+} and Pr^{3+}.

Figures

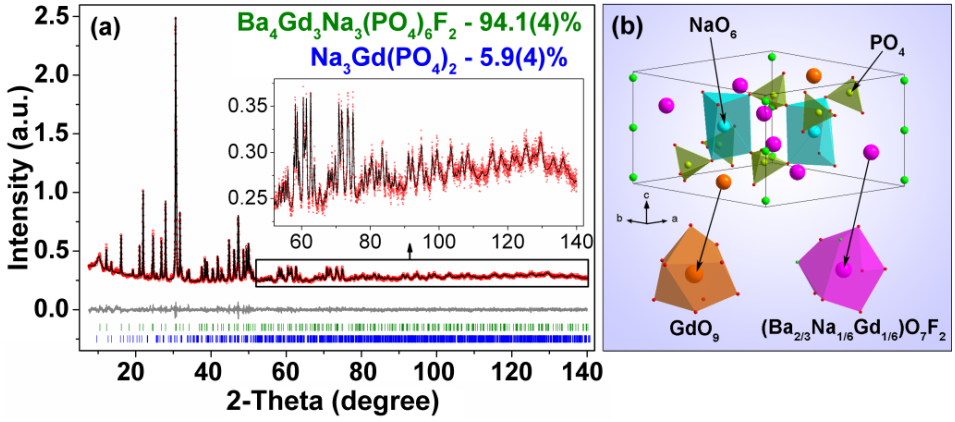

Figure 1. (a) Difference Rietveld plot of $Ba_4Gd_3Na_3(PO_4)_6F_2$ with small amount of $Na_3Gd(PO_4)_2$ impurity; (b) Crystal structure of $Ba_4Gd_3Na_3(PO_4)_6F_2$.

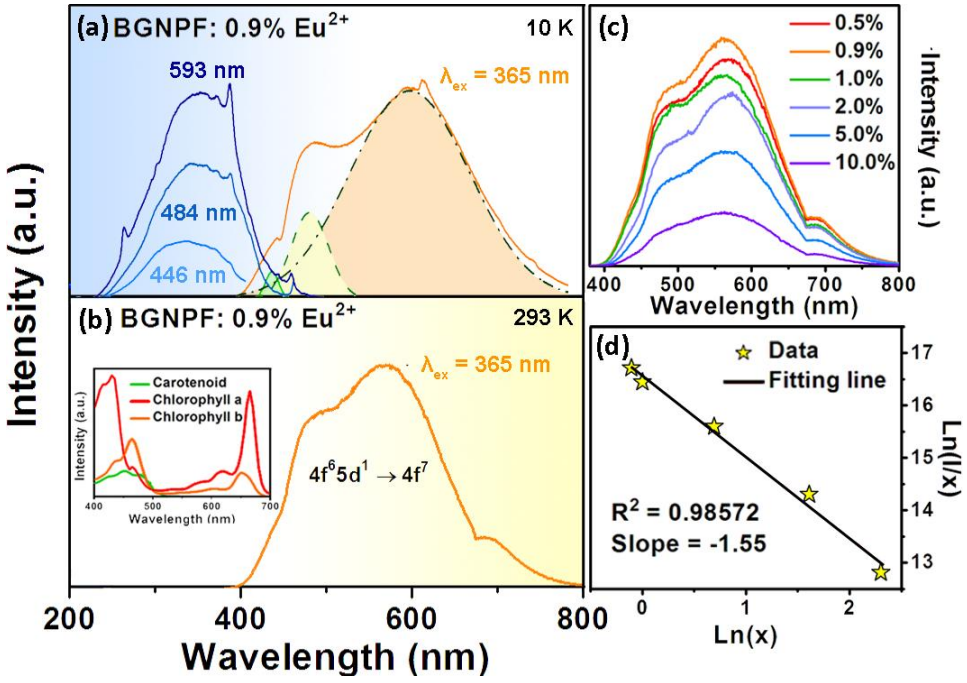

Figure 2. (a) The PLE (λ_{em} = 446, 484, 593 nm) and PL (λ_{ex} = 365 nm) spectra of BGNPF: Eu^{2+} at 10 K and (b) the PL spectra of BGNPF: Eu^{2+} at room temperature; (c) The Eu^{2+} contents-dependent PL spectra of BGNPF: xEu^{2+} (x = 0.5%-10.0%) and (d) The dependence of ln(I/x) on ln(x). The inset of (b) is the absorb spectra of carotenoid, chlorophyll a and b.

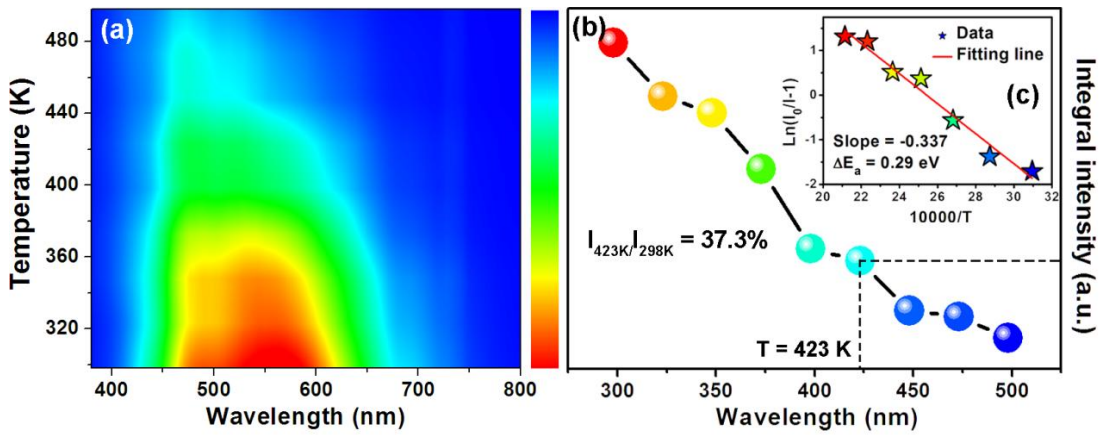

Figure 3. Intensity map of temperature-dependent PL spectra (a) and the corresponding normalized the integrated (400-800 nm) intensity (b) as well as the plot of $\ln(I_0/I\text{-}1)$ *vs* $10000/T$ (c) for sample BGNPF: 0.9%Eu^{2+}.

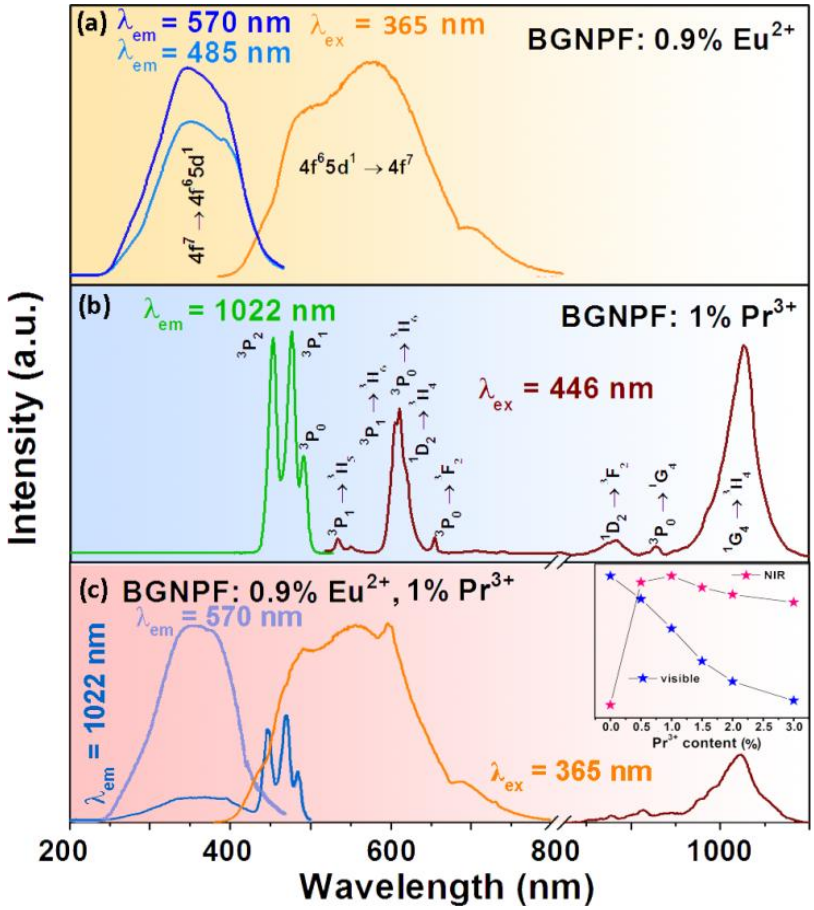

Figure 4. The PLE and PL spectra of (a) BGNPF: 0.9%Eu^{2+}, (b) BGNPF: 1%Pr^{3+} and (c) BGNPF: 0.9%Eu^{2+}, 1%Pr^{3+}.Inset is the Pr^{3+} contents-dependent integral intensity of BGNPF: 0.9%Eu^{2+}, *y*Pr^{3+} samples in visible and NIR region.

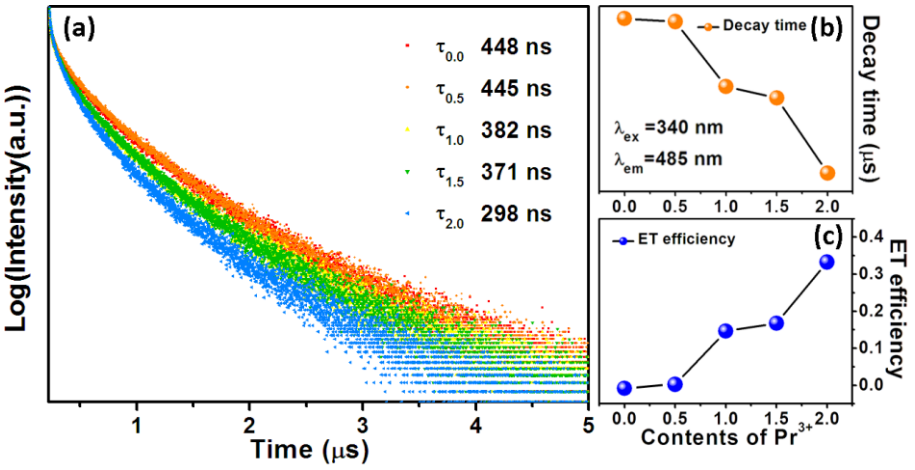

Figure 5. (a) The decay curves, (b) decay time of Eu^{2+} and (c) energy transfer efficiency from Eu^{2+} to Pr^{3+} in phosphor BGNPF: 0.9%Eu^{2+}, *y*Pr^{3+}as function of Pr^{3+} concentration.

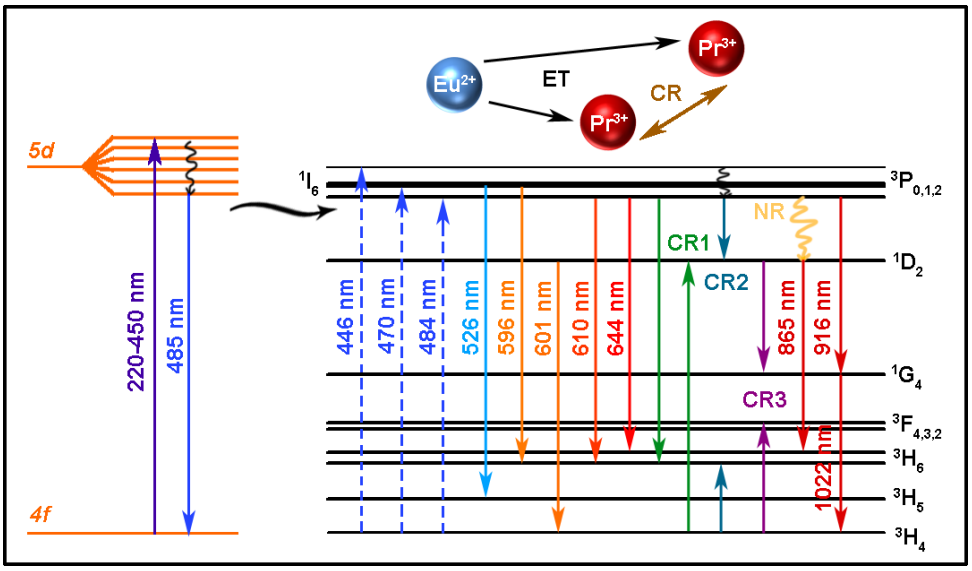

Figure 6. Schematic energy level diagram and the energy transfer process among Eu^{2+} and Pr^{3+}.

Table caption

Table 1. Main parameters of processing and refinement of the $Ba_4Gd_3Na_3(PO_4)_6F_2$ sample.

Table

Table 1. Main parameters of processing and refinement of the $Ba_4Gd_3Na_3(PO_4)_6F_2$ sample.

Compound	**$Ba_4Gd_3Na_3(PO_4)_6F_2$**
Sp. Gr.	*P*-3
a, Å	9.7477 (3)
c, Å	7.2220 (3)
V, Å^3	594.27 (4)
Z	1
R_{wp}, %	2.67
R_p, %	2.05

TABLE OF CONTENTS